Optical fibre-coupled cryogenic radiometer with carbon nanotube absorber

2012 Metrologia 49 S93

(http://iopscience.iop.org/0026-1394/49/2/S93)

Metrologia **49** (2012) S93–S98 doi:10.1088/0026-1394/49/2/S93

Optical fibre-coupled cryogenic radiometer with carbon nanotube absorber

David J Livigni, Nathan A Tomlin, Christopher L Cromer and John H Lehman

Optoelectronics Division, National Institute of Standards and Technology, Boulder, CO 80305-3337, USA

E-mail: livigni@nist.gov

Received 14 September 2011, in final form 22 November 2011
Published 2 March 2012
Online at stacks.iop.org/Met/49/S93

Abstract

A cryogenic radiometer was constructed for direct-substitution optical-fibre power measurements. The cavity is intended to operate at the 3 K temperature stage of a dilution refrigerator or 4.2 K stage of a liquid cryostat. The optical fibre is removable for characterization. The cavity features micromachined silicon centring rings to thermally isolate the optical fibre as well as an absorber made from micromachined silicon on which vertically aligned carbon nanotubes were grown. Measurements of electrical substitution, optical absorption and temperature change indicate that the radiometer is capable of measuring a power level of 10 nW with approximate responsivity of 155 nW K^{-1} and 1/e time constant of 13 min. An inequivalence between optical and electrical power of approximately 10% was found, but the difference was largely attributable to unaccounted losses in the optical fibre.

(Some figures may appear in colour only in the online journal)

1. Introduction

Absolute optical power is measured with high accuracy at NIST by use of collimated laser beams and cryogenic radiometers [1, 2]. Measurement of the optical power delivered through optical fibre is less precise, with a typical uncertainty of 0.5% ($k = 2$) over the power range 10 µW to 200 µW [3]. Optical-fibre power measurements with a lower uncertainty and increased power range, particularly to lower powers, are desired for applications ranging from power-meter manufacturing to research in quantum photonics. An uncertainty of 0.1% ($k = 2$) or less is our target. To achieve the goals of providing lower-uncertainty measurements at the lowest possible power, we developed the Cryogenic Radiometer for Optical Fibre (CROF). In our first design, we maximized responsivity and cavity absorptance with a device that allows the optical fibre to be removed for characterization. The philosophy, construction and performance of the first CROF design are presented here.

2. Heat link

To maximize the CROF's responsivity, we used a polyimide heat link with very low thermal conductivity, and made the length of the heat link the maximum that would fit inside our liquid cryostat. The heat link is shown in an exploded view and photographs in figure 1. We attempt to isolate the removable optical fibre from the heat link to prevent it from providing an alternative heat-flow path. Two concentric polyimide tubes utilizing resistive centring rings provide the isolation. The outermost tube provides the intended heat-flow path, and is the main structural component. The inner polyimide tube holds the optical fibre; it is slightly larger than the fibre, and the fibre fits into the tube with a loose sliding fit.

The inner tube is held within the outer tube by use of centring rings that are designed to resist heat flow. The centring rings, shown in figure 2, are constructed from a micromachined silicon wafer by use of the Bosch process[1] in a commercial deep reactive ion etcher [4]. The centring rings fit inside the outer tube and over the inner tube with sliding fits. The loose fits and features of the centring ring provide resistance to heat flow. The teeth on the inside and outside of the ring reduce the contact area between the ring and tubes, and the right-angle bends in the spokes provide a resistance to low-temperature heat flow. Three centring rings are used. The first ring is recessed a few millimetres from the end of the heat link tube

[1] Certain commercial equipment, instruments or materials are identified in this paper to foster understanding. Such identification does not imply recommendation or endorsement by the National Institute of Standards and Technology, nor does it imply that these products are the best for the purpose specified.

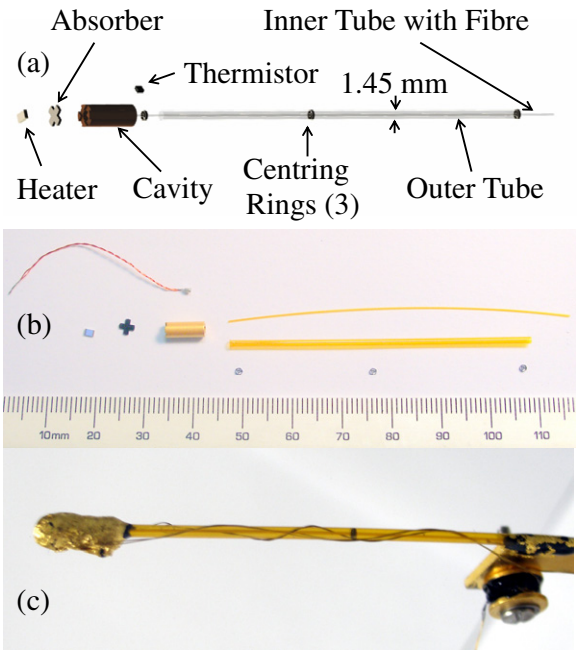

Figure 1. Cryogenic radiometer for optical fibre, (a) details of components, (b) photo of components, (c) photo of assembled radiometer.

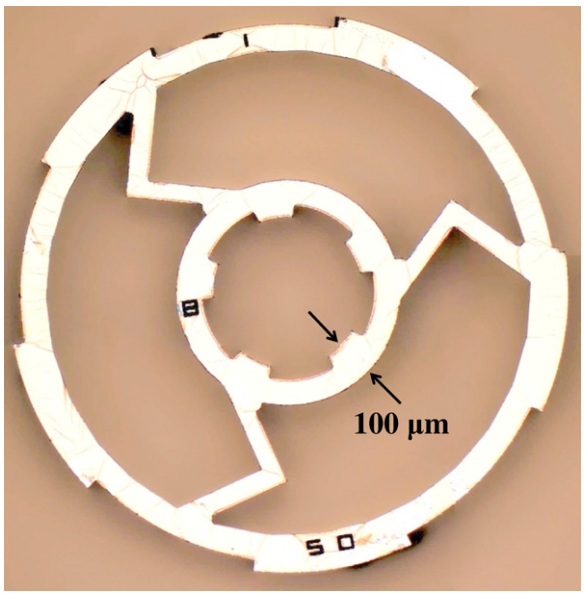

Figure 2. Composite photograph of the silicon centring ring. Nominal ID = 0.38 mm, OD = 1.44 mm and thickness = 0.37 mm.

that connects to the optical cavity. The ring guarantees that the optical fibre is centred in the cavity's aperture. The second ring is in the approximate centre of the heat link and prevents the inner tube from sagging and contacting the outer tube. A third ring is used on the heatsink's end of the heat link, to prevent the tubes from touching. The centring rings are held in place by friction only.

The final element of the heat link is the four superconducting wires that connect to the cavity's temperature sensor and heater. We used niobium–titanium (NbTi) superconducting wire with 70–30 copper–nickel (CuNi) cladding and Heavy Formvar insulation. The wire's cladding layer had a nominal thickness of 0.036 mm. The wires were soldered to the heater and sensor with 50–50 lead–tin solder, and thermally anchored to the cavity with epoxy. Black Stycast 2850 FT epoxy with LV23 hardener was used at a ratio of 13.3 : 1 throughout the construction; the epoxy was exposed to vacuum to remove bubbles, and baked at 65 °C for 2 h in a nitrogen-purged environment to improve adhesion at cryogenic temperatures. From the cavity, the wires were loosely wrapped around the heat link and terminated in copper bobbins that were thermally anchored to the heatsink. Approximately 14 cm of wire was wrapped around the bobbins by use of a bifilar wrap, and encapsulated in epoxy.

On the cavity's end of the heat link, the outer heat link protrudes about 1 mm into the cavity, and is anchored with a small fillet of epoxy. On the heatsink's end, about 1 cm of the tube is epoxied to the heatsink and encapsulated. The inner tube extends for about 1 cm past the outer tube, where it is also encapsulated. Care was taken to leave enough opening in the tubes to allow air to escape the cavity when evacuated. The black epoxy was covered with a layer of gold foil to reduce its emissivity. The optical fibre was thermally anchored behind the heatsink by loosely wrapping the fibre around a copper wire heatsink. For the data presented here, the heat link was connected to a passive heatsink that was bolted directly to the approximately 3 K stage of the dilution refrigerator. When the active heatsink is used, the optical fibre will be thermally anchored about 1 cm behind the inner tube.

The thermal resistance of the contacts at the end of the heat link is unknown. However, the heat flow through the components of the heat link is easily modelled, by use of the relationship $G = kA/L$, where G is the thermal conductance of the element, k is the thermal conductivity of the material that makes up the element, A is the cross-sectional area of the element and L is the length of the element between thermal anchors. The calculated thermal conductivities for the main components of the heat link are shown in table 1. The estimated G's given in the table are rough, because they are derived from estimates of k for similar materials at various temperatures in the range 4 K to 7 K. Contact resistance reduces the estimated G, since the combined G for two conductances in series is the reciprocal of the sum of the reciprocals of each conductance. The combined G for components in parallel is the sum of the G's of the parallel components. Neglecting contact resistance, if we assume that the centring rings effectively isolate the inner tube and fibre optic from the heat-flow path, the combined G for the heat link is the sum of the G's for the outer tube and wires, or 176 nW K^{-1}. If the centring rings failed to provide isolation, the combined G would be 215 nW K^{-1}.

The combined G for the heat link defines the overall responsivity of the radiometer, given here with units of nW K^{-1}. The responsivity must be tailored to the maximum power desired because the allowable temperature rise is limited by the effective superconducting transition temperature of the lead solder to around 7.5 K.

Table 1. Estimated thermal conductance of heat link components at 4 K.

Component	Inner diameter/mm	Outer diameter/mm	Length[a]/mm	Thermal conductivity/nW K^{-1}
Outer polyimide tube	1.450	1.514	50	33
Inner polyimide tube	0.320	0.371	60	5
SMF 28 fibre optic	0	0.245	70	34
Superconducting wire[b]	0	0.107	80	143

[a] Length is the distance between thermal anchors, when present. For the inner tube and fibre, length is the distance from the thermal anchor to the end of the component.
[b] NbTi superconductor with 70/30 CuNi cladding and Formvar insulation, four pieces.

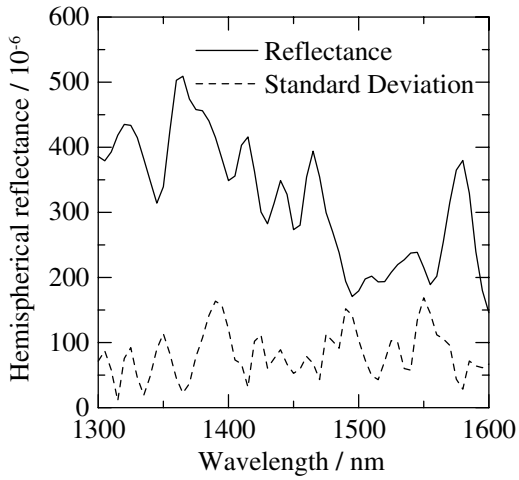

Figure 3. Hemispherical reflectance of 40 µm long vertically aligned carbon nanotubes at common telecommunications wavelengths.

3. Optical cavity

The CROF's optical cavity was designed primarily to maximize the optical absorptance; however, optical–electrical inequivalence, workability and time constant were also concerns. We used a cylindrical optical cavity with sides painted with a glossy black paint, Aeroglaze Z302. A flat optical absorber made of micromachined silicon, coated with vertically aligned carbon nanotubes, was placed at the back of the cavity. It is known that carbon nanotubes are capable of very low reflection [5]. The incident light strikes the absorber at normal incidence. The inside of the cavity has a depth of 7.6 mm and a diameter of 1.5 mm, accounting for the paint thickness and absorber. Calculating the resulting solid angles shows that only 1% of a diffuse back reflection from the absorber would escape the cavity without at least one bounce off the black paint.

An early measurement of the back reflection from the carbon nanotube absorber gave an estimated specular reflection of 0.8%. A more accurate measurement of the hemispherical reflection was performed [6], and additional data acquired that cover the telecommunications wavelengths of interest (1310 nm and 1550 nm) are shown in figure 3. The total uncertainty in the data is unclear because the magnitude of the reflection was unusually low. If we assume figure 3 is accurate, use the worst-case reflection of 500 ppm and apply the worst-case bound that 100% of the reflection is specular and escapes the cavity, we can state that the cavity absorptance is $0.999\,75 \pm 0.000\,29$ ($k = 2$), which is well within the goal of 0.1%. If the actual reflection has a diffuse component, the cavity geometry will result in a higher absorptance.

The inner diameter of the optical cavity was chosen from a set of standard sizes to be a good match for the beam diameter. The 1550 nm wavelength laser beam used in the study was delivered through an SMF 28 optical fibre, which produced a Gaussian beam waist with mode field diameter of 10.4 µm at the tip of the fibre. The beam propagated ~6.6 mm from the fibre to the absorber, where its $1/e^2$ intensity diameter was approximately 1.3 mm—a good fit for a 1.5 mm diameter cavity.

For the body of the cavity, we chose standard C10100 Oxygen Free Electrical (OFE) copper seamless tubing. The standard sized tubing has a nominal inside diameter of 1.549 mm and outside diameter of 3.175 mm. The solid copper tubing was chosen over an electroformed copper cavity for several reasons. We wanted a cavity with good thermal conductivity as determined by its residual resistivity ratio (RRR). Electroformed copper is a hard form of copper with a small grain structure and relatively low RRR. The copper tubing starts as very high RRR copper that becomes work-hardened when drawn and machined, but it is still likely to have a significantly higher RRR than that of electroformed copper. The higher conductivity helps compensate for the greater mass, helping reduce the cavity's time constant. The thickness of the tubing allowed for an easy and effective attachment of the absorber, described below. Also, the tubing can be handled much more roughly than an electroformed part, for example it can be held firmly in a vice without damage or deformation. The work-hardening of the copper tubing could be reversed by annealing the part after machining, before gold plating.

The micromachined silicon wafer that forms the optical absorber has the shape of a plus sign or cross, as shown in figures 1(*a*) and (*b*). The nominal width of the plus sign's arms matched the inside diameter of the copper cavity. Matching notches were machined into the back of the copper cavity before gold plating. Several plus signs with slight variations of the arm widths were manufactured and test-fitted; we selected the plus-sign dimensions that result in a snug press-fit of the plus sign into the cavity, but not so snug as to damage the silicon.

When the optimal size was determined, another set of plus signs with the desired dimensions were manufactured and coated with nanotubes. Vertically aligned multi-wall carbon nanotubes 40 µm long were grown on the absorber by Nanolab,

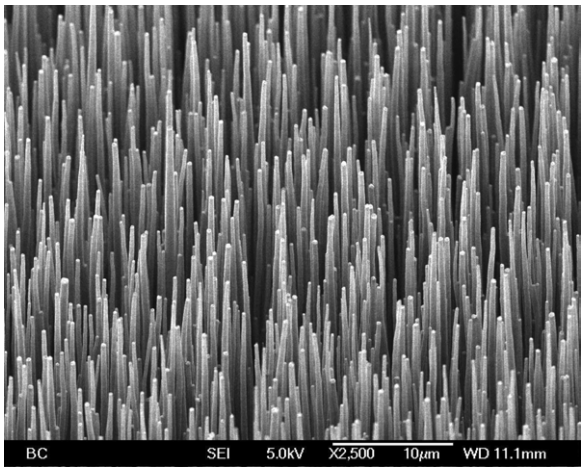

Figure 4. Scanning electron micrograph of the carbon nanotubes on micromachined silicon.

as described elsewhere [7]. A scanning electron micrograph of the nanotube coatings is shown in figure 4. The inside of the cavity was painted, and the coated absorber was pressed into the notches. The nanotubes on the arms of the plus sign are crushed between the micromachined silicon and copper cavity, enhancing the thermal contact. The contact is further enhanced and strengthened by the application of a thin layer of VGE-7031 varnish that fills any gaps, and also cements the heater resistor to the back of the cavity.

The heater was a 1000 Ω Vishay Z-foil resistor, in a 0805 surface mount flip-chip package, having dimensions of 2 mm × 1.25 mm × 0.5 mm. The flip-chip resistor was formed on an alumina substrate with electrical contacts on one side only, so no electrical insulation was required between the substrate and the silicon absorber. The superconducting NbTi wire was soldered to the pads on the front of the resistor before the back of the resistor was glued to the cavity, and the entire assembly was encapsulated in epoxy for strength. The resistor's temperature coefficient is very low, and its resistance changed little from room temperature to 3 K.

We used a silicon thermistor from AdSem Inc. that was optimized for use in the 3 K to 18 K temperature range. The device had dimensions 1 mm × 1 mm × 0.4 mm, and a resistance of approximately 400 kΩ at a temperature of 4 K. Gold leads were attached to the larger faces of the device with indium solder, and the gold leads were spliced to NbTi superconductors a few millimetres from the device. The thermistor was attached to the copper cavity by use of a small square of varnish-soaked cigarette paper for electrical insulation, and the assembly was encapsulated in epoxy for strength.

The thermistor was placed at the front of the cavity, near where it connects to the polyimide heat link. The intent was to place the sensor in a location near where all the electrical and optical heat flux must pass, to minimize the inequivalence between electrical and optical power. However, because the main heat flow in this device was through the wires, the location was not optimal.

The two twisted pairs of wire from the devices were then wrapped once around the cavity and anchored with a small amount of epoxy near the centre of the cavity. The cavity, then mostly covered in black epoxy, was covered in a layer of gold foil to reduce its emissivity. Van der Waals forces were usually sufficient to hold the foil to the cavity, but a small amount of Loctite adhesive was used to enhance the adhesion. The fully assembled cavity is shown in figure 1(*c*). The total mass of the cavity and heat link was 0.62 g, of which 0.41 g was the copper cavity and 0.16 g was epoxy; the balance was the resistor, thermistor, wires and tubes.

4. Experimental setup

The CROF was tested using the 3 K stage of a conventional dilution refrigerator. The wire pairs from the heater and thermometer made four-wire Kelvin connections at the micro-D 25 connector; from there the wires were routed to the outside of the cryostat. The optical fibre followed a similar path, the end of the fibre outside the cryostat was terminated in an FC connector, and the inner end was inserted into the inner polyimide tube of the heat link. A piece of polyimide tape placed on the fibre limited its depth to 7 cm, and friction and the copper wire heatsink held the fibre in place. Additional germanium and silicon sensors were placed on the passive heatsink, and the calibrated germanium resistance thermometer was used to calibrate the silicon thermistors to obtain the absolute temperatures presented here.

The resistance of the sensors was measured with Lakeshore 370 AC Resistance Bridges, with the optional 3708 preamplifier and scanner. A Keithley 2425 Sourcemeter provided the current to heat the cavity's resistor. The applied electrical power was determined by multiplying the square of the applied current by the nominal heater resistance. Given that the current source was not calibrated and the resistance value was nominal, the uncertainty of the electrical power measurement was a few per cent.

Fibre optic power was produced by a tunable laser set to a wavelength of 1550 nm. The light passed through two optical attenuators, and was measured with an Agilent 81634A optical power meter. The desired power was obtained by adjusting the attenuators while reading the power meter. Turning the attenuators to maximum effectively turned off the power. To apply the power to the radiometer, the optical fibre's connector was moved from the power meter to the fibre that connects to the optical cavity, then the attenuators were adjusted to the previously determined levels for the desired power. The power meter was calibrated with an uncertainty of about 1% ($k = 2$). Also, there were unknown losses in the connector and optical fibre leading to the cavity.

5. Experimental results

Open-loop tests were performed, no temperature control was used on the CROF and the cavity temperature was allowed to rise naturally with the applied power. The results of optical and electrical power injections of 1 nW, 3 nW, 10 nW, 30 nW, and 100 nW are shown in figure 5 and detailed in table 2. The response to optical power was roughly 10% lower than that for

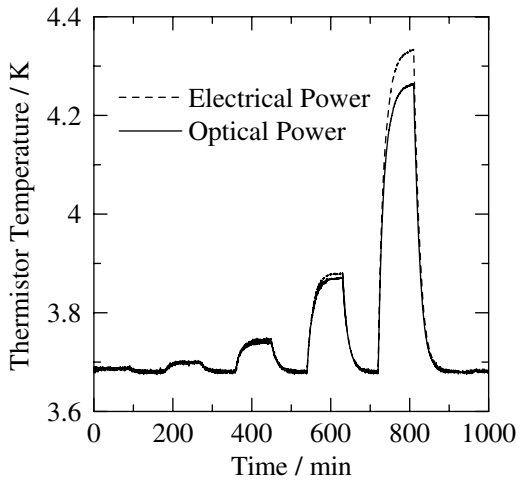

Figure 5. Applied optical and electrical power measurements. Estimated powers were 1 nW, 3 nW, 10 nW, 30 nW and 100 nW.

electrical power, as shown in the inequivalence column of the table. Given the uncertainty in the optical power measurements and unknown loss in the optical fibre and connector, the electrical results are likely more accurate. However, the uncertainty in the electrical and optical measurements is insufficient to explain the large inequivalence measured.

Curves were fitted to the data in figure 5 to determine the steady-state temperature rise and time constant. The temperature rise divided by the applied power determines the device's responsivity G. Since the metallic wires carry most of the heat flux, we fitted a curve appropriate for electron heat transfer and obtained good fits. The time constant results show greater agreement than the responsivity results at comparable power levels, but also appear to change with power. The responsivity results for optical power vary more than the results for electrical power.

6. Conclusions

These experiments with the first CROF cavity show that the technology is capable of performing optical fibre-based optical power measurements at very low powers. However, further development will be necessary before the device is usable for accurate and efficient calibrations. Allowing the device's temperature to rise as in these tests is not a desirable method of calibration; electrical substitution can be performed by reproducing the optical response with electrical power in separate experiments that bracket the optical response, and interpolating. However, this method is very slow and prone to error from drift in source power and background temperature. While the device's long time constant suggests that it could make a good calorimeter, work by West *et al* [8] indicates that treating the device as an isoperibol calorimeter is not appropriate. Challenges include the different fundamental electron and phonon heat-flow modes that are significant at cryogenic temperature, and violate the single exponential decay required by the theory. Another challenge is the significant change in material properties as the temperature rises. Advanced analysis techniques could overcome these factors, but operating the device at a single temperature like a conventional electrical substitution radiometer [1, 2, 9] is a far more elegant solution. Therefore, we are developing a state-of-the-art temperature-control system to use with the device. The device's long time constant complicates operating the device conventionally, since the control system could take a long time to reach steady state. But using an advanced control loop with appropriate feed-forward can reduce the response time; experiments show stability can be achieved in a fraction of the device's natural time constant. So the device should be usable even with its long time constant, although a faster device would be advantageous.

The first CROF was intended to demonstrate the greatest responsivity possible, but the thermal conduction through the wires limited its responsivity. The wire's thermal conductivity could be reduced by etching the CuNi layer off a segment of the wires, or using wires with a thinner CuNi layer, though conduction through the NbTi cores would still be significant at these temperatures. Different lengths, thicknesses and materials of outer tube could be used to tailor the heat link for the desired responsivity and time constant.

The measured responsivity of approximately 155 nW K^{-1} is in good agreement with the estimates of 176 nW K^{-1} and 215 nW K^{-1} for the heat link with and without optical-fibre isolation. Given that adding the contact resistances would lower the estimates, the heat link analysis appears to be accurate. However, since the contact resistances are unknown, the estimates are too uncertain to determine if the optical fibre was effectively isolated. The device's responsivity to electrical power should be measured with and without a fibre inserted to determine how effectively the fibre was isolated.

The optical absorptance of the cavity should be better determined. The cavity itself is too small to perform a conventional integrating sphere measurement [10]. However, the measurement could be performed with a large flat sample of carbon nanotubes to accurately determine the total back reflection from the material from a laser source at normal incidence. The ratio of specular to diffuse reflectance is also needed to accurately model the cavity absorptance. An angled absorber would guarantee that any specular reflection bounces at least once off the paint, but would be much more complicated to manufacture.

The measured results show that the noise level was such that powers of 10 nW or less were clearly resolved; however, there was significant variation in the time constant, responsivity and inequivalence. Some of the variation in the optical power responsivity and inequivalence was likely due to uncertainty in the measurement of optical power and drift. However, the variation with power level in both the optical and electrical time constant and responsivity results were likely due to changes in the material properties as the temperature rose.

The measured inequivalence was too large to be due entirely to uncertainties in the optical and electrical power measurements; it was largely the result of unaccounted losses in the optical fibre that leads to the cavity. The fibre's polished

Table 2. Measured responsivity and time constant for optical and electrical power injections.

	Optical power		Electrical power	
Estimated power/nW	Responsivity/ nW K^{-1}	1/e time constant/min	Responsivity/ nW K^{-1}	1/e time constant/min
1	n/a	n/a	149	12.4
3	160	12.7	149	13.3
10	167	12.1	153	12.9
30	166	13.9	150	13.8
100	171	15	152	15.4

n/a—not available due to bad curve fit.

FC connector can have a loss of 0.3 dB, or about 7%. Also, there were additional unknown bend losses as the fibre snaked its way through the chamber. These losses could account for the entire measured inequivalence, but there is also a mechanism that could cause a true inequivalence between optical and electrical power.

True inequivalence could be the result of the multiple heat-flow paths between the electrical heater and thermistor, the path through the cavity and the path through the wires. The wires are connected through the thermal anchor on the cavity, and there are fewer contact resistances in the path for electrical heating than optical heating. Therefore, proportionally more of the flux from electrical heating may flow through the wires than from optical heating, causing slightly more heating of the thermistor for electrical than for optical power. This inequivalence could be reduced by breaking the heat-flow path through the wires between the heater resistor and thermistor, by not anchoring the wires to the cavity. Removing the thermal anchor may increase the period needed for the wire segments to cool to their critical temperature, but should otherwise cause no problems.

Acknowledgment

The authors thank Dr Chris Chunnilall of NPL for the carbon nanotube reflectance measurements.

References

[1] Livigni D 2003 NIST Special Publication 250-62
[2] Houston J M and Rice J P 2006 *Metrologia* **43** S31–5
[3] Vayshenker I, Li X, Livigni D J, Scott T R and Cromer C L 2000 NIST Special Publication 250-54
[4] Laermer F and Urban A 2003 *Microelectron. Eng.* **67–68** 349–55
[5] Lehman J, Sanders A, Hanssen L, Wilthan B, Zeng J and Jensen C 2010 *Nano Lett.* **10** 3261–6
[6] Chunnilall C J, Lehman J H and Theocharous E 2011 *Proc. NEWRAD (Maui, HI)* pp 122–3
[7] Lehman J H, Lee B and Grossman E N 2011 *Appl. Opt.* **50** 4099–104
[8] West E D and Churney K L 1970 *J. Appl. Phys.* **41** 2705–12
[9] Datla R U, Stock K, Parr A C, Hoytm C C, Miller P J and Foukal P V 1992 *Appl. Opt.* **31** 7219–25
[10] Touayar O, Rougie B, Coutin J M and Bastie J 1998 *Metrologia* **35** 387–91